
A Boundary-Layer Mechanism for One-Third Scaling in Online Softmax Classification

Marcel Kühn^{1,2,*} Yoon Thelge¹ Bernd Rosenow^{1,2}
¹Institute for Theoretical Physics, Leipzig University
²ScaDS.AI Dresden/Leipzig

Abstract

Hard-label classification is usually trained with smooth surrogate losses, most prominently softmax cross-entropy. We isolate an asymptotic mechanism by which this mismatch between smooth surrogate and discrete labels produces power-law learning curves in an online teacher-student model. After subtracting the mean logit, the thermodynamic-limit dynamics close in centered variables: a growing centered student-teacher alignment D and the residual student variance Δ . At late times, examples away from teacher decision boundaries are already classified confidently and contribute exponentially little. Only boundary layers of width $O(D^{-1})$ remain active, while the noise of fixed-learning-rate online gradient descent maintains a nonzero Δ . As a function of the training time α the late-time solution yields a $\alpha^{-1/3}$ power law not only for the test loss but also for the generalization error ϵ_g , i.e., one minus test accuracy. This is much slower than the α^{-1} Bayes-optimal reference for the same model. We further show that learning-rate schedules can improve the generalization error towards a $\epsilon_g \sim \alpha^{-1/2}$ power law. Simulations support the predicted order parameter dynamics and learning curves. Controlled experiments with correlated Gaussian inputs and whitened pretrained features show that data structure can dominate transients. Therefore, our result is an asymptotic, complementary mechanism rather than an alternative to spectral explanations of neural scaling laws.

1 Introduction

Scaling laws make learning dynamics predictable: they summarize how error decreases with data, compute, model size, or optimization time. Empirical work has made such laws central to modern machine learning [1–4]. A major theoretical route explains these laws from structure in the data distribution, target function, or feature map. In kernel, random-feature, and linear models, power-law spectra of feature or data covariance matrices can be converted into power-law learning curves [5–9]; related geometric considerations connect exponents to the effective dimension of the data manifold [10, 11]. Feature-learning analyses show how these spectral mechanisms can change once the representation evolves during training [12–14].

Power laws can also arise from mechanisms that are not primarily spectral. Simplified sequence-modeling models show how scaling behavior can emerge without explicit power-law correlations in the data [15], while recent work shows that softmax and cross-entropy can intrinsically produce one-third time scaling when learning peaked probability distributions [16]. High-dimensional teacher-student theories provide another complementary viewpoint, with precise learning curves for multiclass classification under Bayes-optimal and empirical-risk minimization procedures, including cross-entropy loss [17]. Here we isolate a different late-time mechanism: a leading-order boundary-layer realization of the softmax/cross-entropy bottleneck in online hard-label classification.

*Corresponding author: mkuehn@itp.uni-leipzig.de

This motivates a focused question: what controls the late-time learning dynamics of online multiclass classification when the labels are discrete but the student is trained through differentiable probabilities? We study this question in a one-layer K -class teacher-student model with Gaussian inputs and online stochastic gradient descent (SGD), using the order-parameter methodology of the statistical physics of learning [18–20]. The model is simple enough to solve in the thermodynamic limit, but rich enough to expose an asymptotic mechanism that is easy to miss in the raw order parameters.

Our contributions. We derive an exact centered macroscopic closure for symmetric online K -class softmax learning. We then give a boundary-layer derivation of the softmax/cross-entropy bottleneck in hard-label classification, compute the leading classification-error asymptotics, and show how a learning-rate schedule can improve them. We confirm the theory with finite-dimensional simulations and use controlled departures from the isotropic Gaussian setting as mechanism tests. See Fig. 1 for an overview.

The main observation is that the late-time dynamics becomes transparent only after removing a redundancy of the softmax. Adding the same constant to every logit does not change the predicted probabilities, so the common mean is irrelevant. The natural coordinates are therefore centered quantities: the alignment of a student class vector with its own teacher relative to its alignment with other teachers, and the squared length of a student class vector relative to its overlap with other student vectors. Denoting these by the centered overlap D and the centered norm Q_{eff} , we define the residual student variance as $\Delta = Q_{\text{eff}} - D^2$, which comes from fluctuations of the student orthogonal to the teacher.

In these variables, perfect learning is not convergence to a finite-weight fixed point. Instead, the centered overlap D grows without bound, while at fixed learning rate the residual variance Δ approaches a finite noise floor. The only examples that remain active lie within $O(D^{-1})$ of pairwise teacher decision boundaries. The shrinking measure of these active boundary layers gives $\dot{D} \propto D^{-2}$, and therefore $D \sim \alpha^{1/3}$. The classification error is controlled by the angle between centered student and teacher, $\epsilon_g \propto \sqrt{\Delta}/D$, giving $\epsilon_g \propto \sqrt{\Delta}/D$, giving

$$\epsilon_g(\alpha) \sim \alpha^{-1/3}. \quad (1)$$

Annealing the learning rate changes the residual noise floor. For a slowly decaying learning rate $\eta(\alpha) \propto \alpha^{-\gamma}$ with $0 \leq \gamma < 1$, this gives $\epsilon_g(\alpha) \sim \alpha^{-(2+\gamma)/6}$; in the limit $\gamma \rightarrow 1$, the generalization error improves toward $\epsilon_g \sim \alpha^{-1/2}$. This rate remains slower than Bayes-optimal rates in related high-dimensional theories, but mirrors reports for cross-entropy minimization on static datasets [17]. A companion calculation for a smooth perceptron classifier trained on hard labels with mean-squared-error loss, given in Section D, shows that the same asymptotic learning curves, together with a diverging norm, a shrinking angle, and an online-noise floor, can extend beyond the softmax/cross-entropy surrogate.

The results should be read in the context of Liu et al. [16], who show that softmax and cross-entropy can generate one-third scaling when learning peaked distributions. We do not claim that the exponent $1/3$ is unique to the present model. The contribution is a statistical-mechanics realization of this bottleneck for online hard-label classification: the centered closure localizes the slow drift geometrically, computes the misclassification asymptotics, and separates deterministic boundary-layer motion from stochastic online-SGD noise.

Assumptions and scope. All asymptotic claims are made for the permutation-symmetric online teacher–student model defined below, with the thermodynamic limit taken before the late-time limit. The analysis is a population online-SGD result: each update sees a fresh draw from the input distribution, not a repeated pass over a finite training set. The main formulas are stated for fixed K as the thermodynamic limit $N \rightarrow \infty$ is taken. The noiseless hard-label assumption is also essential: soft targets, label noise, or irreducible Bayes error can create bulk gradients or an error floor that masks the boundary-layer asymptote. The paper therefore does not claim to explain all neural scaling laws. It isolates one solvable late-time mechanism for fixed-feature, online, hard-label classification with a smooth surrogate.

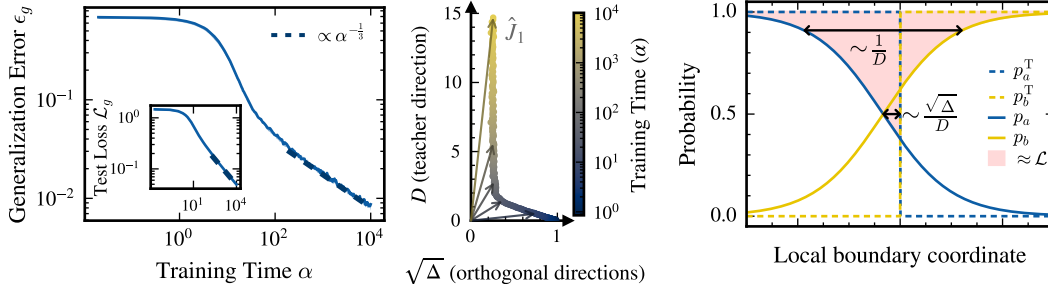


Figure 1: Left: The 1/3 law appears not only in the test loss but also in the generalization error ϵ_g , i.e., one minus test accuracy. Middle: The model captures both the growth of the centered student-teacher alignment D and the rotational alignment to the teacher. Right: Near a teacher decision boundary, the late-time loss is controlled by the student boundary layer of width $O(D^{-1})$. The generalization error is controlled by residual boundary fluctuations only of order $\sqrt{\Delta}/D$.

2 Related work

Empirical scaling laws have motivated a broad set of theoretical explanations, including spectral, geometric, and feature-learning mechanisms [5–8, 10, 12–14]. Our work is complementary: it gives a sharply scoped classification example in which decision-boundary geometry and online optimization noise produce a power law even without a structured input spectrum.

The closest recent result is the one-third softmax and cross-entropy bottleneck of Liu et al. [16]. They analyze the learning of peaked target distributions, where probability mass is concentrated on a small number of coordinates. In their model, the growth of the student norm leads to a 1/3 power law for the test loss; they also support this scaling with empirical evidence from large-language-model training. The corresponding development of rotational alignment between student and teacher, however, is not resolved by that analysis. Hard labels are a limiting case of peaked targets, so our fixed-learning-rate exponent should be viewed as part of the same phenomenon. The distinction is that the present hard-label teacher-student setting closes exactly in centered variables. This closure identifies the active set as pairwise teacher decision-boundary layers, allows us to compute the classification-error prefactor, and makes explicit the roles of online-SGD noise and learning-rate annealing. Thus the present model explains not only test loss scaling through growth of the student norm, but also classification-error scaling through the rotational alignment of student and teacher.

The analysis uses the classic teacher–student and thermodynamic-limit methodology of the statistical physics of learning [18–21]. In this tradition, high-dimensional stochastic learning dynamics reduce to deterministic flows for self-averaging order parameters. Power-law late-time behavior can also arise from dynamical degeneracies in online teacher–student models, for example through soft modes in over-realizable soft committee machines [22]. Modern work has extended these ideas to richer neural-network and high-dimensional classification settings [23–25]. The key mathematical step in the present manuscript is the centered multiclass reduction: the raw variables R, S, Q, C are useful scaffolding, but the softmax dynamics and classification asymptotics are naturally expressed in $D = R - S$ and $Q_{\text{eff}} = Q - C$.

High-dimensional teacher–student analyses provide reference points for Bayes-optimal classification, convex optimization, and learning curves with generic feature maps [17, 26, 27]. These works address the asymptotic performance of estimators trained on a static set of examples, whereas the present paper addresses late-time online dynamics for hard-label classification under softmax and cross-entropy updates. The whitened-feature experiments in Section 6 use pretrained vision-transformer (ViT) representations as a controlled non-Gaussian test bed [28]. They are robustness checks of the boundary-layer mechanism, not a theory of representation learning.

Our results also connect to smooth surrogate losses and implicit bias. Calibration and consistency theory relates surrogate risk to classification risk [29, 30], and recent work gives universal square-root rates for smooth surrogate-loss H -consistency bounds [31]. The limiting behavior of our annealing schedule, improving toward $\epsilon_g(\alpha) \sim \alpha^{-1/2}$, echoes this square-root behavior but concerns online optimization time rather than excess-risk transforms. For separable data, gradient descent on logistic

or cross-entropy losses drives weights toward max-margin directions while the norm diverges [32]. Related work studies fixed-learning-rate SGD and multiclass extensions of this implicit-bias picture [33–35]. Our population online setting differs because fresh examples continually inject boundary noise, leaving a residual uncertainty at fixed learning rate that annealing can reduce.

More broadly, the paper follows the use of physics-inspired analytic models to understand machine-learning behavior, complementary to physics-informed machine-learning methods that build physical constraints into models [36]. We do not argue that data structure or representation learning are irrelevant. Rather, we isolate an optimization-and-classification mechanism already present in an analytically clean fixed-feature model.

3 Centered online dynamics for the K -class softmax student

3.1 Teacher-student model and centered order parameters

We study a single-layer student that maps N -dimensional inputs to K logits, one for each class. The labels are generated by a teacher network. Let $T_1, \dots, T_K \in \mathbb{R}^N$ be orthogonal teacher vectors, normalized as $T_a \cdot T_b / N = \delta_{ab}$, where δ_{ab} is the Kronecker delta. Inputs $\xi \in \mathbb{R}^N$ are standard Gaussian. The teacher fields and one-hot labels are

$$u_a = \frac{T_a \cdot \xi}{\sqrt{N}}, \quad p_a^\top = \mathbf{1}\{u_a = \max_b u_b\}, \quad (2)$$

where $\mathbf{1}\{\cdot\}$ is the indicator function. Ties have probability zero under the Gaussian input distribution. The student has weights J_1, \dots, J_K , with logits and softmax probabilities

$$t_a = \frac{J_a \cdot \xi}{\sqrt{N}}, \quad p_a = \frac{e^{t_a}}{\sum_{b=1}^K e^{t_b}}. \quad (3)$$

For a single example, the cross-entropy loss is $\mathcal{L} = -\log p_y$, where y is the teacher label. Online gradient descent with learning rate η gives the update

$$J_a^{\mu+1} = J_a^\mu + \frac{\eta}{\sqrt{N}} (p_a^{\top, \mu} - p_a^\mu) \xi^\mu, \quad \alpha = \frac{\mu}{N}. \quad (4)$$

We take $N \rightarrow \infty$ at fixed K and fixed macroscopic time α , and then study the large- α asymptotics under a permutation-symmetric ansatz. The same formulas extend to slowly growing K only in the regime where pairwise boundary layers remain dominant; see Section 4.

Under permutation symmetry between classes, the standard statistical mechanics order parameters are

$$R = \frac{J_1 \cdot T_1}{N}, \quad S = \frac{J_1 \cdot T_2}{N}, \quad Q = \frac{J_1 \cdot J_1}{N}, \quad C = \frac{J_1 \cdot J_2}{N}. \quad (5)$$

By symmetry, the choice of indices is arbitrary, with 1 and 2 denoting distinct classes. Here R is the overlap with the matching teacher, S is the overlap with a non-matching teacher, Q is the student norm, and C is the overlap between two distinct student weight vectors.

The softmax probabilities are invariant under a common shift of the logits, $t_a \mapsto t_a + c$. The mean logit is therefore dynamically irrelevant. This motivates the centered order parameters

$$D := R - S, \quad Q_{\text{eff}} := Q - C, \quad \Delta := Q_{\text{eff}} - D^2. \quad (6)$$

Their geometric meaning is transparent in centered coordinates. Define the centered student $\hat{J}_a := \sqrt{\frac{K}{K-1}}(J_a - \bar{J})$ and centered teacher $\hat{T}_a := \sqrt{\frac{K}{K-1}}(T_a - \bar{T})$ with $\bar{T} := \frac{1}{K} \sum_a T_a$ and $\bar{J} := \frac{1}{K} \sum_a J_a$. Then, for any class a ,

$$D = \frac{\hat{J}_a \cdot \hat{T}_a}{N}, \quad Q_{\text{eff}} = \frac{\hat{J}_a \cdot \hat{J}_a}{N}. \quad (7)$$

Thus D is the centered student-teacher overlap, Q_{eff} is the centered student norm, and Δ is the residual student variance due to fluctuations of the student orthogonal to the teacher.

3.2 Exact closure in D and Δ

For the macroscopic dynamics, only the centered student logits and teacher fields matter. In the thermodynamic limit, their joint Gaussian law can be represented as

$$h_a := t_a - \bar{t} = D(u_a - \bar{u}) + \sqrt{\Delta}(z_a - \bar{z}), \quad (8)$$

where $\bar{t} = K^{-1} \sum_a t_a$, $\bar{u} = K^{-1} \sum_a u_a$, $\bar{z} = K^{-1} \sum_a z_a$, and the z_a are auxiliary i.i.d. standard Gaussians independent of the teacher fields. The first term is the centered teacher-aligned signal, with scale D . The second term is residual centered noise, with scale $\sqrt{\Delta}$. Since the softmax probabilities depend only on the centered logits h_a , this representation is used throughout the paper, simplifying the analysis by considering uncorrelated Gaussian variables u_a and z_a .

Let $p_a^\top = \mathbf{1}\{u_a = \max_b u_b\}$ and $g_a = p_a^\top - p_a$. In the thermodynamic limit, the permutation-symmetric online learning process closes exactly on the centered variables. With dots denoting derivatives with respect to α , the centered alignment obeys $\dot{D} = \frac{K}{K-1} \eta \langle g_1(u_1 - \bar{u}) \rangle$, where the average is over the Gaussian fields in Eq. (8). The centered norm evolves as $\dot{Q}_{\text{eff}} = \frac{K}{K-1} (2\eta \langle g_1 h_1 \rangle + \eta^2 \langle g_1^2 \rangle)$, with the first term coming from deterministic drift and the second from online-SGD noise. Finally, since $\Delta = Q_{\text{eff}} - D^2$, its time derivative is $\dot{\Delta} = \dot{Q}_{\text{eff}} - 2D\dot{D}$.

No late-time approximation has been made up to this point. In the thermodynamic limit, the stochastic online dynamics has reduced to a deterministic closed flow for the centered overlap and residual variance. The derivation from the microscopic update, including the centered Gaussian representation, is given in Section A.

4 Boundary layers control the late-time regime

Almost-perfect learning. The self-consistent late-time regime is $D \rightarrow \infty$ and $\Delta = O(1)$. In this regime, the signal term in Eq. (8) is large except near teacher decision boundaries. Away from boundaries, the teacher and student agree exponentially well, and examples make exponentially small contributions to the macroscopic flow. For fixed K , the leading contributions therefore come from pairwise boundary layers of width $O(D^{-1})$ around $u_a = u_b$; higher-order ties are lower-dimensional sets and are subleading. For growing K , the same reduction requires $D \gg \sqrt{2 \log K}$ (see Section B.1).

For a fixed pair $a \neq b$, the boundary is locally relevant only when the other $K - 2$ teacher fields lie below the common value. This gives the geometric boundary density

$$c_K := \int_{-\infty}^{\infty} \varphi(s)^2 \Phi(s)^{K-2} ds, \quad (9)$$

where φ and Φ are the standard normal density and distribution function. All dependence on the number of classes enters the asymptotic prefactors through this boundary density and the number of pairwise boundaries.

Local binary reduction. Near one active boundary, scale the teacher gap as $u_a - u_b = \frac{x}{D}$. Then the corresponding centered student-logit gap has the form

$$h_a - h_b = x + \delta, \quad \delta = \sqrt{2\Delta} z, \quad z \sim \mathcal{N}(0, 1). \quad (10)$$

All other classes are exponentially suppressed at leading order, so the local softmax comparison is binary. The universal local update is $\Theta(x) - \sigma(x + \delta)$ with $\sigma(y) = 1/(1 + e^{-y})$. The only non-elementary scalar function that remains is

$$\mathcal{B}(\Delta) = \int Dz \left[2 \log \left(2 \cosh \left(\sqrt{\frac{\Delta}{2}} z \right) \right) - 1 \right], \quad Dz = \frac{e^{-z^2/2}}{\sqrt{2\pi}} dz. \quad (11)$$

For small Δ , $\mathcal{B}(\Delta) = 2 \log 2 - 1 + \Delta/2 + O(\Delta^2)$.

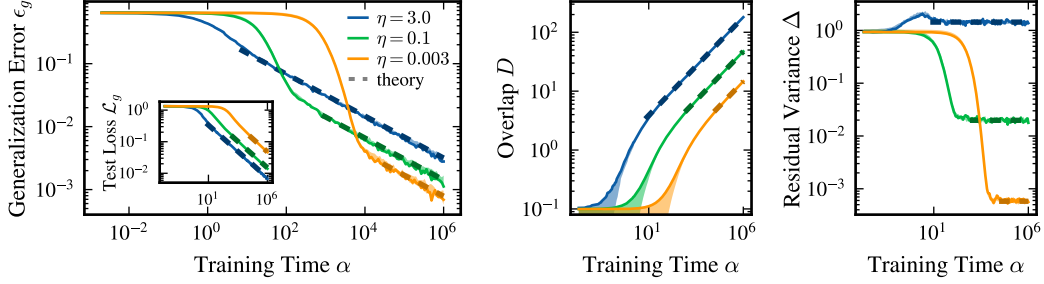


Figure 2: Finite- N validation for fixed learning rates in the $K = 3$ online teacher–student model. The panels show the generalization error, centered overlap D , and residual variance Δ as functions of macroscopic time $\alpha = \mu/N$. The curves show representative seed trajectories, with envelopes indicating fluctuations across six simulation seeds. Within these fluctuations, the trajectories agree with the predicted power-law prefactors and exponents: $D \sim \alpha^{1/3}$, Δ approaches a learning-rate-dependent floor, and $\epsilon_g \propto \sqrt{\Delta}/D \sim \alpha^{-1/3}$; see Eqs. (14) and (16).

Asymptotic reduced flow. Applying the local reduction to the exact closure gives, for fixed K and $D \rightarrow \infty$, the leading late-time equations

$$\dot{D} = \frac{Kc_K}{2} \frac{\eta(\alpha)}{D^2} \left(\frac{\pi^2}{6} + \Delta \right) + o(D^{-2}), \quad (12)$$

$$\dot{\Delta} = \frac{Kc_K}{D} [\eta(\alpha)^2 \mathcal{B}(\Delta) - 2\eta(\alpha)\Delta] + o(D^{-1}). \quad (13)$$

The structure of these equations gives the mechanism. The factor D^{-2} in \dot{D} comes from the shrinking measure of the active boundary layers and the local antisymmetry of the update. The $\eta^2 \mathcal{B}(\Delta)$ term in $\dot{\Delta}$ is the surviving online-SGD noise. Thus fixed-learning-rate dynamics does not drive Δ to zero; it drives Δ to a noise floor while D continues to grow.

For constant η , Eq. (13) has the fixed point $2\Delta_* = \eta \mathcal{B}(\Delta_*)$. Substituting this into Eq. (12) gives

$$D(\alpha) \sim \left[\frac{3Kc_K}{2} \eta \left(\frac{\pi^2}{6} + \Delta_* \right) \right]^{1/3} \alpha^{1/3}, \quad \Delta \simeq \Delta_*. \quad (14)$$

Generalization error. The classification generalization error is

$$\epsilon_g := \Pr \left[\arg \max_a h_a \neq \arg \max_a u_a \right]. \quad (15)$$

It is governed by the same boundary layers. Locally, a teacher-student disagreement occurs when the signs of x and $x + \delta$ differ. Averaging the length of this disagreement interval and summing over unordered class pairs gives

$$\epsilon_g = \Gamma_K \frac{\sqrt{\Delta}}{D} + o(D^{-1}), \quad \Gamma_K = \frac{K(K-1)c_K}{\sqrt{\pi}}. \quad (16)$$

Prediction 1: fixed learning rate. Combining Eqs. (14) and (16) yields the fixed-learning-rate prediction

$$D \sim \alpha^{1/3}, \quad \Delta \simeq \Delta_*, \quad \epsilon_g \sim \alpha^{-1/3}. \quad (17)$$

Within the solvable model, the exponent is therefore not a consequence of a data spectrum. It follows from the boundary-layer drift $\dot{D} \propto D^{-2}$ together with a finite residual online-noise scale. The details of the full late-time boundary-layer evaluation are given in Section B.

5 Exponents with learning rate schedules

Taking a smaller fixed learning rate lowers the asymptotic noise floor, but it also delays entry into the asymptotic regime; see Fig. 2. Learning-rate schedules can improve the asymptotic error exponent

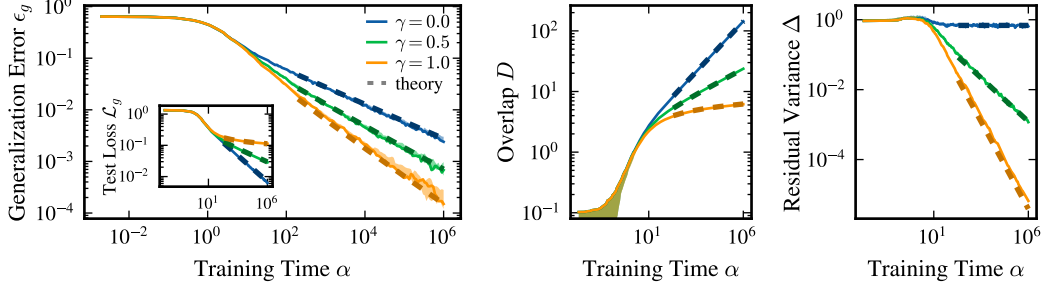


Figure 3: Schedule dependence in the $K = 3$ online teacher–student model. For $\eta(\alpha) \propto \alpha^{-\gamma}$, the theory predicts $\epsilon_g(\alpha) \sim \alpha^{-(2+\gamma)/6}$ for $0 \leq \gamma < 1$. Increasing γ slows the growth of the centered overlap, $D \propto \alpha^{(1-\gamma)/3}$ for $\gamma < 1$, but decreases the residual variance, $\Delta \propto \eta(\alpha)$; the latter effect improves the classification-error exponent. The $\gamma = 1$ curve is a borderline case, where the adiabatic approximation for Δ breaks down. For reference, the adiabatic predictions of Eqs. (19) and (20) are also shown.

because they allow the residual variance Δ to decrease while the accumulated learning time continues to grow.

Suppose $\eta(\alpha) \rightarrow 0$ slowly enough that Δ adiabatically tracks the instantaneous fixed point of Eq. (13). Using the small- Δ expansion of \mathcal{B} gives $\Delta(\alpha) \sim \kappa \eta(\alpha)$ with $\kappa = (2 \log 2 - 1)/2$. Then Eq. (12) reduces to $\dot{D} \sim \frac{K c_K \pi^2}{12} \frac{\eta(\alpha)}{D^2}$. With

$$H(\alpha) = \int_0^\alpha \eta(\alpha') d\alpha', \quad (18)$$

one obtains

$$D(\alpha) \sim \left(\frac{K c_K \pi^2}{4} H(\alpha) \right)^{1/3}, \quad \Delta \sim \kappa \eta(\alpha). \quad (19)$$

Prediction 2: scheduled learning rates. Together with Eq. (16), this gives the general schedule prediction

$$\epsilon_g(\alpha) \sim A_K \frac{\sqrt{\eta(\alpha)}}{H(\alpha)^{1/3}}, \quad A_K = \Gamma_K \sqrt{\kappa} \left(\frac{4}{K c_K \pi^2} \right)^{1/3}. \quad (20)$$

For the power-law schedule $\eta(\alpha) \sim \alpha^{-\gamma}$ with $0 \leq \gamma < 1$, this gives $\epsilon_g(\alpha) \sim \alpha^{-(2+\gamma)/6}$. The exponent therefore interpolates continuously from $1/3$ at $\gamma = 0$ toward $1/2$ as $\gamma \uparrow 1$. For $\gamma = 1$, the relaxation of Δ is no longer fast enough to track $\Delta_*(\alpha) \propto \eta(\alpha)$. Thus the exponent $1/2$ is approached from below within the adiabatic family, but is not attained by the borderline schedule itself. If $\gamma > 1$, the integral $H(\alpha)$ converges and the centered overlap stops growing, so asymptotically perfect learning is lost.

Thus, within this online-SGD and adiabatic-schedule class, annealing moves the asymptotic error from the fixed- η $1/3$ law toward a borderline near- $1/2$ law. This should be read as a statement about the analyzed training family, not as a universal optimization ceiling for all possible algorithms. The adiabatic schedule derivation, together with the corresponding cross-entropy test-loss asymptotics, is collected in Section C.

6 Numerical validation and controlled departures

The simulations are designed as mechanism tests, not as evidence for a universal empirical scaling law. Within the solvable model, they check whether the three quantities that appear in the asymptotic theory behave consistently with the slow manifold: the centered overlap should grow, the residual variance should either approach a fixed learning-rate-dependent floor or track the learning-rate schedule, and the error should be controlled by the ratio $\sqrt{\Delta}/D$. We then use correlated Gaussian inputs and whitened pretrained features as controlled departures from the assumptions of the derivation.

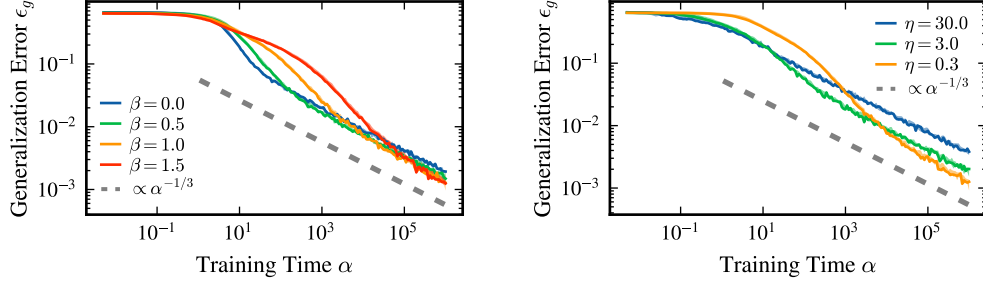


Figure 5: Controlled departure from isotropic inputs. Inputs are Gaussian with diagonal covariance spectrum $\langle \xi_i^2 \rangle \sim i^{-\beta}$, normalized so that the largest variance is one. Left: $\eta = 0.5$ is fixed and β is varied. Right: $\beta = 1.0$ is fixed and the learning rate is varied. Increasing β changes and lengthens the transient regime. The late-time decay remains consistent with the same boundary-layer asymptote, while smaller learning rates reduce asymptotic prefactors but can delay entry into the asymptotic regime.

Further numerical details, additional fixed-learning-rate sweeps, and the real-label whitened-feature comparison are reported in Section E.

For fixed learning rate, the theory predicts more than a slope for ϵ_g . It predicts the internal structure of the trajectory: D grows without bound, Δ relaxes to a residual noise floor, and $\epsilon_g \propto \sqrt{\Delta}/D$. The test loss \mathcal{L}_g also shows a power-law decay. In particular, we compare the simulations with Eqs. (14) and (16) and with the test-loss prediction in Eq. (60) of Section B.4. The finite- N simulations in Fig. 2 agree well with these predictions. Larger learning rates enter the scaling regime earlier but leave a larger residual variance, while smaller learning rates reduce the asymptotic floor but can delay the onset of the late-time behavior. Additional simulations confirming the K -dependence of the predictions are shown in Section E.1.

The schedule sweep in Fig. 3 tests the same mechanism in a different way. Annealing reduces the online-noise floor, so the residual variance Δ decreases with the learning rate as predicted by Eq. (19). At the same time, the accumulated learning time $H(\alpha)$ grows more slowly, which slows the growth of D , again as predicted by Eq. (19). The observed improvement of the error exponent is therefore not a separate effect.

It comes from the competition between slower overlap growth and faster variance suppression, as summarized by Eq. (20). The corresponding test-loss scaling follows from Eq. (77); the loss decays more slowly when the growth of D is slowed. The $\gamma = 1$ curve is the borderline case where the adiabatic argument for Δ is not asymptotically valid. We nevertheless show the main-text adiabatic prediction as a finite-time reference. Over the range displayed, it remains a good guide and the generalization error shows a near- $1/2$ power law.

The correlated-Gaussian experiment in Fig. 5 probes a different vulnerability of the theory. The derivation assumes isotropic inputs, whereas structured spectra can dominate the early learning dynamics. The simulations suggest that this structure mainly modifies the crossover: larger β produces longer transients, but the later error decay remains consistent with the boundary-layer prediction. This supports the interpretation that covariance structure and boundary-layer dynamics can control different time windows.

Finally, Fig. 5 asks whether the same late-time pattern is visible when the Gaussian assumption is relaxed but the covariance is controlled. The teacher-label run is consistent with the same qualitative

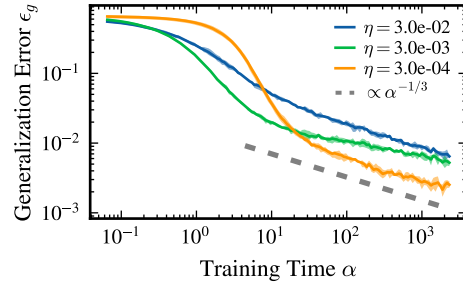


Figure 5: Non-Gaussian robustness test using whitened pretrained features. A linear softmax readout is trained online on whitened ViT features with teacher-generated labels. Whitening controls the covariance, while the feature distribution remains non-Gaussian. The teacher-generated labels avoid an early real-label performance floor and allow the late-time regime to be observed.

scaling picture, suggesting that the mechanism is not immediately destroyed by non-Gaussian feature statistics. The corresponding real-label run, shown in Fig. 7 in Section E, reaches a floor much earlier. We interpret this as a limitation of the model. For real labels, aspects such as model misspecification, label noise, or irreducible Bayes error can dominate the late-time error before the noiseless boundary-layer asymptote is cleanly visible.

Taken together, the simulations support the mechanism inside the solvable setting and probe several controlled departures from it. They also emphasize a practical point: transients can be long, and the learning rate that is best at a finite training horizon need not be the one with the best asymptotic prefactor.

7 Discussion and scope

We have identified a boundary-layer mechanism for late-time online hard-label classification trained with softmax and cross-entropy in a solvable fixed-feature teacher-student model. The essential step is to use centered variables. In these variables, learning is controlled by a diverging centered margin D and a residual variance Δ . For fixed learning rate, online gradient noise keeps Δ finite, while only $O(D^{-1})$ -thin decision-boundary layers remain active. This produces $D \sim \alpha^{1/3}$ and $\epsilon_g \sim \alpha^{-1/3}$.

The relationship to recent one-third scaling results should be interpreted carefully. Liu et al. [16] identify a broad softmax and cross-entropy bottleneck for learning peaked distributions, using a perfectly aligned student–teacher model, and support the loss-scaling prediction with empirical evidence from large-language-model training. The present paper gives a complementary, narrower result: in online hard-label classification, the bottleneck can be localized geometrically at teacher decision boundaries, evaluated asymptotically in centered order parameters, and connected directly to the misclassification probability through the rotational alignment of student and teacher. The schedule law is the main additional dynamical consequence. Annealing reduces the residual variance and leads to power-law learning curves that interpolate between the fixed-learning-rate $1/3$ law and a borderline near- $1/2$ law. This remains slower than the α^{-1} Bayes-optimal rate in related teacher–student settings, but mirrors reports for cross-entropy minimization on static datasets [17].

The scope is intentionally limited. The theory assumes a one-layer readout, fixed features, online SGD with fresh examples, a thermodynamic limit, noiseless hard labels, and a permutation-symmetric teacher–student setting. It does not claim that data structure is irrelevant, nor that feature learning cannot change the asymptotic class. Indeed, the correlated-input experiments show that structured covariance can strongly affect transients. Soft targets, label noise, or irreducible Bayes error create further limitations by introducing bulk gradients or performance floors that can mask the noiseless hard-label boundary-layer regime.

These limitations suggest concrete extensions. A soft-teacher or noisy-label version of the centered closure would connect the present theory to Bayes-error floors in real data. Minibatching and momentum should modify the online-noise term in the Δ equation. Richer optimizers may change the range of useful learning-rate schedules. Feature-learning architectures could couple the boundary-layer dynamics of the readout to changes in the representation. The present work provides a baseline for those questions: a solvable classification scaling law whose exponent is generated by decision-boundary geometry and online optimization noise.

References

- [1] Joel Hestness, Sharan Narang, Newsha Ardalani, Gregory Diamos, Heewoo Jun, Hassan Kianinejad, Md. Mostofa Ali Patwary, Yang Yang, and Yanqi Zhou. Deep Learning Scaling is Predictable, Empirically. *arXiv preprint arXiv:1712.00409*, 2017.
- [2] Jordan Hoffmann, Sebastian Borgeaud, Arthur Mensch, Elena Buchatskaya, Trevor Cai, Eliza Rutherford, Diego de Las Casas, Lisa Anne Hendricks, Johannes Welbl, Aidan Clark, Thomas Hennigan, Eric Noland, Katherine Millican, George van den Driessche, Bogdan Damoc, Aurelia Guy, Simon Osindero, Karén Simonyan, Erich Elsen, Oriol Vinyals, Jack Rae, and Laurent Sifre. An empirical analysis of compute-optimal large language model training. In S. Koyejo, S. Mohamed, A. Agarwal, D. Belgrave, K. Cho, and A. Oh, editors, *Advances in Neural Information Processing Systems*, volume 35, pages 30016–30030. Curran Associates, Inc., 2022.

- [3] Jared Kaplan, Sam McCandlish, Tom Henighan, Tom B. Brown, Benjamin Chess, Rewon Child, Scott Gray, Alec Radford, Jeffrey Wu, and Dario Amodei. Scaling Laws for Neural Language Models. *arXiv preprint arXiv:2001.08361*, 2020.
- [4] Jack W. Rae et al. Scaling Language Models: Methods, Analysis & Insights from Training Gopher. *arXiv preprint arXiv:2112.11446*, 2021.
- [5] Blake Bordelon, Abdulkadir Canatar, and Cengiz Pehlevan. Spectrum dependent learning curves in kernel regression and wide neural networks. In *Proceedings of the 37th International Conference on Machine Learning*, volume 119 of *Proceedings of Machine Learning Research*, pages 1024–1034. PMLR, 2020.
- [6] Abdulkadir Canatar, Blake Bordelon, and Cengiz Pehlevan. Spectral bias and task-model alignment explain generalization in kernel regression and infinitely wide neural networks. *Nature Communications*, 12(1): 2914, 2021.
- [7] Yasaman Bahri, Ethan Dyer, Jared Kaplan, Jaehoon Lee, and Utkarsh Sharma. Explaining neural scaling laws. *Proceedings of the National Academy of Sciences*, 121(27):e2311878121, 2024.
- [8] Alexander Maloney, Daniel A. Roberts, and James Sully. A solvable model of neural scaling laws. *arXiv preprint arXiv:2210.16859*, 2022.
- [9] Licong Lin, Jingfeng Wu, Sham M. Kakade, Peter L. Bartlett, and Jason D. Lee. Scaling laws in linear regression: Compute, parameters, and data. *Advances in Neural Information Processing Systems*, 37, 2024.
- [10] Utkarsh Sharma and Jared Kaplan. Scaling laws from the data manifold dimension. *Journal of Machine Learning Research*, 23(9):1–34, 2022.
- [11] Ryotaro Nakada and Masaaki Imaizumi. Adaptive approximation and generalization of deep neural networks with intrinsic dimensionality. *Journal of Machine Learning Research*, 21(174):1–38, 2020.
- [12] Blake Bordelon, Alexander Atanasov, and Cengiz Pehlevan. A dynamical model of neural scaling laws. In *International Conference on Machine Learning*, 2024.
- [13] Blake Bordelon, Alexander Atanasov, and Cengiz Pehlevan. How feature learning can improve neural scaling laws. *Journal of Statistical Mechanics: Theory and Experiment*, 2025(8):084002, 2025.
- [14] Roman Worschech and Bernd Rosenow. Analyzing neural scaling laws in two-layer networks with power-law data spectra. In *International Conference on Learning Representations*, 2025. Spotlight.
- [15] Maissam Barkeshli, Alberto Alfarano, and Andrey Gromov. On the origin of neural scaling laws: From random graphs to natural language. *arXiv preprint arXiv:2601.10684*, 2026.
- [16] Yizhou Liu, Ziming Liu, Cengiz Pehlevan, and Jeff Gore. Universal One-third Time Scaling in Learning Peaked Distributions. *arXiv preprint arXiv:2602.03685*, 2026.
- [17] Elisabetta Cornacchia, Francesca Mignacco, Rodrigo Veiga, Cédric Gerbelot, Bruno Loureiro, and Lenka Zdeborová. Learning curves for the multi-class teacher–student perceptron. *Machine Learning: Science and Technology*, 4(1):015019, 2023.
- [18] Michael Biehl and Peter Riegler. On-line learning with a student-teacher scenario. *Europhysics Letters*, 28(7):525, 1994.
- [19] Manfred Opper and David Haussler. Calculation of the learning curve of bayes optimal classification algorithm for learning a perceptron with noise. *Physical Review Letters*, 66(20):2677, 1991.
- [20] David Saad and Sara A Solla. Exact solution for on-line learning in multilayer neural networks. *Physical Review Letters*, 74(21):4337, 1995.
- [21] H. S. Seung, H. Sompolinsky, and N. Tishby. Statistical mechanics of learning from examples. *Phys. Rev. A*, 45:6056–6091, Apr 1992.
- [22] Frederieke Richert, Roman Worschech, and Bernd Rosenow. Soft mode in the dynamics of over-realizable online learning for soft committee machines. *Physical Review E*, 105(5):L052302, 2022.
- [23] Madhu S Advani and Andrew M Saxe. High-dimensional dynamics of generalization error in neural networks. *Neural Networks*, 132:428–446, 2020.
- [24] Sebastian Goldt, Madhu Advani, Andrew M Saxe, Florent Krzakala, and Lenka Zdeborová. Dynamics of stochastic gradient descent for two-layer neural networks in the teacher-student setup. In *Advances in Neural Information Processing Systems*, volume 32, 2019.

- [25] Francesca Mignacco, Florent Krzakala, Pierfrancesco Urbani, and Lenka Zdeborová. Dynamical mean-field theory for sgd in high-dimensional classification. In *Advances in Neural Information Processing Systems*, volume 33, pages 5834–5845, 2020.
- [26] Benjamin Aubin, Florent Krzakala, Yue Lu, and Lenka Zdeborová. Generalization error in high-dimensional perceptrons: Approaching bayes error with convex optimization. *Advances in Neural Information Processing Systems*, 33:12199–12210, 2020.
- [27] Bruno Loureiro, Gabriele Sicuro, Cédric Gerbelot, Alessandro Pocco, Florent Krzakala, and Lenka Zdeborová. Learning curves of generic features maps for realistic datasets with a teacher-student model. In *Advances in Neural Information Processing Systems*, volume 34, pages 18137–18151, 2021.
- [28] Alexey Dosovitskiy, Lucas Beyer, Alexander Kolesnikov, Dirk Weissenborn, Xiaohua Zhai, Thomas Unterthiner, Mostafa Dehghani, Matthias Minderer, Georg Heigold, Sylvain Gelly, Jakob Uszkoreit, and Neil Houlsby. An image is worth 16x16 words: Transformers for image recognition at scale. In *International Conference on Learning Representations*, 2021.
- [29] Tong Zhang. Statistical behavior and consistency of classification methods based on convex risk minimization. *The Annals of Statistics*, 32(1):56–134, 2004.
- [30] Peter L. Bartlett, Michael I. Jordan, and Jon D. McAuliffe. Convexity, classification, and risk bounds. *Journal of the American Statistical Association*, 101(473):138–156, 2006.
- [31] Anqi Mao, Mehryar Mohri, and Yutao Zhong. A Universal Growth Rate for Learning with Smooth Surrogate Losses. In *Advances in Neural Information Processing Systems*, volume 37, pages 41670–41708. Curran Associates, Inc., 2024.
- [32] Daniel Soudry, Elad Hoffer, Mor Shpigel Nacson, Suriya Gunasekar, and Nathan Srebro. The implicit bias of gradient descent on separable data. In *International Conference on Learning Representations*, 2018.
- [33] Mor Shpigel Nacson, Nathan Srebro, and Daniel Soudry. Stochastic gradient descent on separable data: Exact convergence with a fixed learning rate. In *Proceedings of the Twenty-Second International Conference on Artificial Intelligence and Statistics*, volume 89 of *Proceedings of Machine Learning Research*, pages 3051–3059. PMLR, 2019.
- [34] Yutong Wang and Clayton Scott. Unified binary and multiclass margin-based classification. *Journal of Machine Learning Research*, 25(143):1–51, 2024.
- [35] Hrithik Ravi, Clayton Scott, Daniel Soudry, and Yutong Wang. The implicit bias of gradient descent on separable multiclass data. In *Advances in Neural Information Processing Systems*, volume 37, 2024.
- [36] Maziar Raissi, Paris Perdikaris, and George E Karniadakis. Physics-informed neural networks: A deep learning framework for solving forward and inverse problems involving nonlinear partial differential equations. *Journal of Computational physics*, 378:686–707, 2019.
- [37] Preetum Nakkiran, Behnam Neyshabur, and Hanie Sedghi. The deep bootstrap framework: Good online learners are good offline generalizers. In *International Conference on Learning Representations*, 2021.

A Exact centered dynamics for the symmetric K -class model

This appendix gives the derivation of the exact centered closure used in Section 3. Throughout, K is fixed while $N \rightarrow \infty$. The teacher fields $u_a = T_a \cdot \xi / \sqrt{N}$ are i.i.d. standard Gaussians, and the student logits are $t_a = J_a \cdot \xi / \sqrt{N}$. Under the permutation-symmetric ansatz, the macroscopic state is described by

$$R = \frac{J_1 \cdot T_1}{N}, \quad S = \frac{J_1 \cdot T_2}{N}, \quad Q = \frac{J_1 \cdot J_1}{N}, \quad C = \frac{J_1 \cdot J_2}{N}. \quad (21)$$

The online update is

$$J_a^{\mu+1} = J_a^\mu + \frac{\eta}{\sqrt{N}} g_a \xi^\mu, \quad g_a = p_a^T - p_a, \quad p_a^T = \mathbf{1}\{u_a = \max_b u_b\}. \quad (22)$$

Since one update changes the order parameters by $O(N^{-1})$, the thermodynamic limit with $\alpha = \mu/N$ gives deterministic flows. From Eq. (22),

$$\dot{R} = \eta \langle g_1 u_1 \rangle, \quad (23)$$

$$\dot{S} = \eta \langle g_1 u_2 \rangle, \quad (24)$$

$$\dot{Q} = 2\eta \langle g_1 t_1 \rangle + \eta^2 \langle g_1^2 \rangle, \quad (25)$$

$$\dot{C} = \eta \langle g_1 t_2 + g_2 t_1 \rangle + \eta^2 \langle g_1 g_2 \rangle. \quad (26)$$

Here and below, brackets denote averages over the jointly Gaussian teacher and student fields at fixed order parameters.

A.1 Centered Gaussian representation

Let

$$\bar{u} = \frac{1}{K} \sum_{a=1}^K u_a, \quad \bar{t} = \frac{1}{K} \sum_{a=1}^K t_a, \quad h_a = t_a - \bar{t}. \quad (27)$$

The teacher labels and the softmax probabilities are invariant under common shifts of the teacher fields and student logits, so the averages in the exact flow depend only on the centered variables $u_a - \bar{u}$ and h_a . It is therefore enough to characterize their joint Gaussian law, which under the symmetric ansatz is fully specified by D and Δ . The centered teacher variables $u_a - \bar{u}$ span the same $(K-1)$ -dimensional subspace as the softmax logits. A direct covariance calculation using Eq. (21) gives

$$\mathbb{E}[h_a | u_1, \dots, u_K] = D(u_a - \bar{u}), \quad (28)$$

and the residual centered covariance is proportional to the centered projector. Hence the centered logits admit the representation

$$h_a = D(u_a - \bar{u}) + \sqrt{\Delta} (z_a - \bar{z}), \quad \Delta = Q_{\text{eff}} - D^2, \quad (29)$$

where z_a are i.i.d. standard Gaussians independent of the u_a and $\bar{z} = K^{-1} \sum_a z_a$. This is the representation used in the main text.

A.2 Exact centered closure

Subtracting Eq. (24) from Eq. (23) gives

$$\dot{D} = \eta \langle g_1 (u_1 - u_2) \rangle. \quad (30)$$

Equivalently, using the independence of the common teacher mode,

$$\dot{D} = \frac{K}{K-1} \eta \langle g_1 (u_1 - \bar{u}) \rangle. \quad (31)$$

Using the identities $\sum_a g_a = 0$ and $\sum_a h_a = 0$, the norm equation reduces to

$$\dot{Q}_{\text{eff}} = \frac{K}{K-1} [2\eta \langle g_1 h_1 \rangle + \eta^2 \langle g_1^2 \rangle]. \quad (32)$$

Finally,

$$\dot{\Delta} = \dot{Q}_{\text{eff}} - 2D\dot{D}. \quad (33)$$

Equations (31)–(33) are exact in the thermodynamic limit under the symmetric ansatz. The boundary-layer analysis below is an asymptotic evaluation of their Gaussian averages.

B Boundary-layer derivation for the K -class softmax model

We now derive Eqs. (12), (13) and (16). The self-consistent almost-perfect-learning regime is

$$D \rightarrow \infty, \quad \Delta = O(1). \quad (34)$$

Away from teacher decision boundaries, the deterministic part $D(u_a - \bar{u})$ of the centered logits separates the correct class by an $O(D)$ margin, and the residual $O(1)$ noise cannot change the

class except with exponentially small probability. Thus the leading dynamics comes from $O(D^{-1})$ neighborhoods of pairwise boundaries. The boundary-layer regime is reached by for large D , but the required value of D increases with K . The two largest Gaussian teacher fields are typically separated by only $O(1/\sqrt{2\log K})$, so the corresponding student-logit gap is $O(D/\sqrt{2\log K})$. Thus the classes are determined exponentially well away from decision boundaries under the condition $D \gg \sqrt{2\log K}$.

B.1 Boundary density and top-gap distribution

Fix an unordered pair $\{a, b\}$. On the boundary $u_a = u_b = s$, the other $K - 2$ teacher fields must lie below s for this pair to be the locally competing top pair. The single-pair boundary density is therefore

$$c_K = \int_{-\infty}^{\infty} \varphi(s)^2 \Phi(s)^{K-2} ds, \quad (35)$$

where

$$\varphi(s) = \frac{e^{-s^2/2}}{\sqrt{2\pi}}, \quad \Phi(s) = \int_{-\infty}^s \varphi(x) dx. \quad (36)$$

The classification-error prefactor uses unordered boundaries and hence $K(K - 1)/2$ pairs.

B.2 Universal local binary integrals

Near one active boundary, set

$$u_a - u_b = \frac{x}{D}. \quad (37)$$

Then the student-logit gap is

$$h_a - h_b = x + \delta, \quad \delta = \sqrt{2\Delta} z, \quad z \sim \mathcal{N}(0, 1). \quad (38)$$

All remaining classes are lower by an $O(D)$ margin at leading order. Hence the local softmax reduces to the binary logistic comparison

$$\Theta(x) - \sigma(x + \delta), \quad \sigma(y) = \frac{1}{1 + e^{-y}}. \quad (39)$$

The following identities are used repeatedly:

$$A_0(\delta) := \int_{-\infty}^{\infty} [\Theta(x) - \sigma(x + \delta)] dx = -\delta, \quad (40)$$

$$A_1(\delta) := \int_{-\infty}^{\infty} x [\Theta(x) - \sigma(x + \delta)] dx = \frac{\delta^2}{2} + \frac{\pi^2}{6}, \quad (41)$$

$$A_2(\delta) := \int_{-\infty}^{\infty} (x + \delta) [\Theta(x) - \sigma(x + \delta)] dx = \frac{\pi^2}{6} - \frac{\delta^2}{2}, \quad (42)$$

$$B_0(\delta) := \int_{-\infty}^{\infty} [\Theta(x) - \sigma(x + \delta)]^2 dx = 2 \log \left(2 \cosh \frac{\delta}{2} \right) - 1. \quad (43)$$

Averaging over $\delta = \sqrt{2\Delta} z$ gives, with $Dz = (2\pi)^{-1/2} e^{-z^2/2} dz$,

$$\int Dz A_1(\sqrt{2\Delta} z) = \frac{\pi^2}{6} + \Delta, \quad (44)$$

$$\int Dz A_2(\sqrt{2\Delta} z) = \frac{\pi^2}{6} - \Delta, \quad (45)$$

$$\mathcal{B}(\Delta) := \int Dz B_0(\sqrt{2\Delta} z) = \int Dz \left[2 \log \left(2 \cosh \left(\sqrt{\frac{\Delta}{2}} z \right) \right) - 1 \right]. \quad (46)$$

For small Δ ,

$$\mathcal{B}(\Delta) = 2 \log 2 - 1 + \frac{\Delta}{2} + O(\Delta^2). \quad (47)$$

B.3 Asymptotic order-parameter flow

Applying the boundary-layer scaling to Eq. (31), the constant part of the local centered teacher coordinate cancels after the x integration; the first nonzero term is the linear part in the gap. Summing the equal contributions from the $K - 1$ boundaries adjacent to class 1 yields

$$\dot{D} = \frac{Kc_K}{2} \frac{\eta(\alpha)}{D^2} \left(\frac{\pi^2}{6} + \Delta \right) + o(D^{-2}). \quad (48)$$

Likewise, the drift part of Eq. (32) gives the A_2 integral, while the online-noise part gives the B_0 integral. Thus

$$\dot{Q}_{\text{eff}} = \frac{Kc_K}{D} \left[\eta(\alpha) \left(\frac{\pi^2}{6} - \Delta \right) + \eta(\alpha)^2 \mathcal{B}(\Delta) \right] + o(D^{-1}). \quad (49)$$

Combining Eqs. (48) and (49) with $\dot{\Delta} = \dot{Q}_{\text{eff}} - 2D\dot{D}$ gives

$$\dot{\Delta} = \frac{Kc_K}{D} \left[\eta(\alpha)^2 \mathcal{B}(\Delta) - 2\eta(\alpha)\Delta \right] + o(D^{-1}). \quad (50)$$

For constant learning rate, Δ relaxes to the fixed point

$$2\Delta_* = \eta \mathcal{B}(\Delta_*). \quad (51)$$

Then

$$D^3(\alpha) \sim \frac{3Kc_K}{2} \eta \left(\frac{\pi^2}{6} + \Delta_* \right) \alpha, \quad (52)$$

and therefore

$$D \sim \alpha^{1/3}, \quad Q_{\text{eff}} \sim \alpha^{2/3}, \quad \frac{\sqrt{\Delta_*}}{D} \sim \alpha^{-1/3}. \quad (53)$$

B.4 Generalization error and test loss

The misclassification probability is

$$\epsilon_g = \Pr \left[\arg \max_a h_a \neq \arg \max_a u_a \right]. \quad (54)$$

Near an unordered boundary $\{a, b\}$, a mistake occurs exactly when x and $x + \delta$ have opposite signs. For fixed δ , the length of the disagreement interval is $|\delta|$. Hence

$$\epsilon_g = \frac{K(K-1)c_K}{2} \frac{1}{D} \mathbb{E}|\delta| + o(D^{-1}). \quad (55)$$

Since $\delta \sim \mathcal{N}(0, 2\Delta)$, $\mathbb{E}|\delta| = 2\sqrt{\Delta/\pi}$, and

$$\epsilon_g = \Gamma_K \frac{\sqrt{\Delta}}{D} + o(D^{-1}), \quad \Gamma_K = \frac{K(K-1)c_K}{\sqrt{\pi}}. \quad (56)$$

Together with Eq. (53), this gives $\epsilon_g \sim \alpha^{-1/3}$ for fixed η .

The same local reduction also gives the population cross-entropy test loss,

$$\mathcal{L}_g = \mathbb{E}[-\log p_y]. \quad (57)$$

For a local boundary and fixed δ , the loss integral is

$$\mathcal{L}_0(\delta) = \int_0^\infty \log(1 + e^{-x-\delta}) dx + \int_0^\infty \log(1 + e^{-x+\delta}) dx \quad (58)$$

$$= \frac{\pi^2}{6} + \frac{\delta^2}{2}. \quad (59)$$

After averaging over $\delta = \sqrt{2\Delta}z$ and summing unordered boundaries,

$$\mathcal{L}_g = \frac{K(K-1)c_K}{2D} \left(\frac{\pi^2}{6} + \Delta \right) + o(D^{-1}). \quad (60)$$

Thus for fixed learning rate the population cross-entropy loss decays as $D^{-1} \sim \alpha^{-1/3}$. Under annealing with $\Delta \rightarrow 0$, the leading loss scales as $H(\alpha)^{-1/3}$ rather than as the classification error; this explains why optimizing the classification-error exponent and optimizing the loss exponent need not be identical.

C Learning-rate schedules

We derive the schedule law used in Section 5. For slowly decaying $\eta(\alpha)$, and as long as the residual variance can adiabatically follow the instantaneous fixed point of Eq. (50), one obtains the following schedule law. Since

$$\mathcal{B}(\Delta) = 2 \log 2 - 1 + \frac{\Delta}{2} + O(\Delta^2), \quad (61)$$

the fixed point satisfies

$$\Delta(\alpha) \sim \kappa \eta(\alpha), \quad \kappa = \frac{2 \log 2 - 1}{2}. \quad (62)$$

Substituting Eq. (62) into Eq. (48) gives

$$\dot{D} \sim \frac{K c_K \pi^2 \eta(\alpha)}{12 D^2}. \quad (63)$$

With

$$H(\alpha) = \int_0^\alpha \eta(\alpha') d\alpha', \quad (64)$$

integration yields

$$D^3(\alpha) \sim \frac{K c_K \pi^2}{4} H(\alpha). \quad (65)$$

Combining Eqs. (56), (62) and (65) gives

$$\epsilon_g(\alpha) \sim A_K \frac{\sqrt{\eta(\alpha)}}{H(\alpha)^{1/3}}, \quad A_K = \Gamma_K \sqrt{\kappa} \left(\frac{4}{K c_K \pi^2} \right)^{1/3}. \quad (66)$$

For numerical stability near $\alpha = 0$, the experiments use the shifted power-law schedule

$$\eta(\alpha) = \eta_0 \left(1 + \frac{\alpha}{\alpha_0} \right)^{-\gamma}. \quad (67)$$

For $0 \leq \gamma < 1$,

$$H(\alpha) \sim \frac{\eta_0 \alpha_0}{1 - \gamma} \left(1 + \frac{\alpha}{\alpha_0} \right)^{1-\gamma}. \quad (68)$$

Therefore the adiabatic schedule law gives

$$\epsilon_g(\alpha) \sim A_K (1 - \gamma)^{1/3} \eta_0^{1/6} \alpha_0^{\gamma/6} \alpha^{-(2+\gamma)/6}. \quad (69)$$

This is self-consistent for every fixed $0 \leq \gamma < 1$. Indeed, the relaxation rate of Δ around the instantaneous fixed point is

$$\lambda(\alpha) \sim \frac{2K c_K}{D(\alpha)} \eta(\alpha). \quad (70)$$

Using $D(\alpha) \sim H(\alpha)^{1/3}$, one obtains

$$\lambda(\alpha) \alpha \sim \alpha^{2(1-\gamma)/3} \rightarrow \infty, \quad 0 \leq \gamma < 1. \quad (71)$$

Thus the relaxation time of Δ is asymptotically shorter than the time scale over which the schedule changes.

The borderline schedule $\gamma = 1$ is singular. In this case

$$\eta(\alpha) \sim \alpha_0^{-1}, \quad H(\alpha) \sim \log \alpha, \quad (72)$$

and hence

$$D(\alpha) \sim (\log \alpha)^{1/3}. \quad (73)$$

The relaxation rate is then

$$\lambda(\alpha) \sim \frac{1}{\alpha(\log \alpha)^{1/3}}, \quad (74)$$

up to a positive constant. Hence $\lambda(\alpha)\alpha \rightarrow 0$, and the adiabatic tracking assumption fails at asymptotically late times.

Equivalently, writing the small- Δ equation in the form

$$\dot{\Delta} \sim -\lambda(\alpha)\Delta + \lambda(\alpha)\kappa\eta(\alpha), \quad (75)$$

the homogeneous part gives

$$\Delta(\alpha) = C_\Delta \exp\left[-b_\Delta(\log \alpha)^{2/3}\right], \quad b_\Delta > 0. \quad (76)$$

This solution is self-consistent for large α , because the omitted instantaneous-fixed-point scale $\kappa\eta(\alpha) \propto \alpha^{-1}$ decays faster than $\Delta(\alpha)$. Therefore also the generic borderline classification error decays slower than for any fixed $\gamma = 1 - \varepsilon$ schedule. Thus the exponent 1/2 is approached only as a limiting adiabatic exponent for $\gamma \uparrow 1$, not by the borderline schedule itself.

The test-loss formula Eq. (60) gives the corresponding leading loss behavior

$$\mathcal{L}_g(\alpha) \sim \frac{K(K-1)c_K \pi^2}{2D(\alpha)} \frac{1}{6} \propto H(\alpha)^{-1/3} \quad (77)$$

whenever $\eta(\alpha) \rightarrow 0$ and $D(\alpha)$ continues to diverge. In particular, for $0 \leq \gamma < 1$ one has

$$\mathcal{L}_g(\alpha) \sim \alpha^{-(1-\gamma)/3}, \quad (78)$$

while the borderline schedule gives

$$\mathcal{L}_g(\alpha) \sim (\log \alpha)^{-1/3}. \quad (79)$$

For $\gamma > 1$, $D(\alpha)$ saturates, and the test loss does not vanish asymptotically.

D Binary warmup: smooth student for a hard teacher

This appendix records the simpler binary mechanism used as a warmup. It is not needed for the K -class proof, but it shows that the same qualitative ingredients—a diverging norm, a shrinking angle, and an online-noise floor—also appear outside the softmax model.

Let $T, J \in \mathbb{R}^N$ and define

$$u = \frac{T \cdot \xi}{\sqrt{N}}, \quad t = \frac{J \cdot \xi}{\sqrt{N}}. \quad (80)$$

The teacher label is $\tau(u) = \text{sgn}(u)$ and the student output is

$$g(t) = \text{erf}\left(\frac{t}{\sqrt{2}}\right). \quad (81)$$

For squared loss $\mathcal{L} = (\tau(u) - g(t))^2/2$, online gradient descent gives

$$J^{\mu+1} = J^\mu + \frac{\eta}{\sqrt{N}}[\tau - g(t)]g'(t)\xi^\mu. \quad (82)$$

With

$$Q = \frac{J \cdot J}{N}, \quad \rho = \frac{J \cdot T}{N}, \quad R = \frac{\rho}{\sqrt{Q}}, \quad (83)$$

the fields $(u, t/\sqrt{Q})$ are standard correlated Gaussians with correlation R . The thermodynamic-limit flow is

$$\frac{d\rho}{d\alpha} = \frac{2\eta}{\pi(Q+1)} \left[\sqrt{Q - \rho^2 + 1} - \frac{\rho}{\sqrt{2Q+1}} \right], \quad (84)$$

$$\begin{aligned} \frac{dQ}{d\alpha} = & \frac{4\eta}{\pi(Q+1)} \left[\frac{\rho}{\sqrt{Q - \rho^2 + 1}} - \frac{Q}{\sqrt{2Q+1}} \right] \\ & + \frac{2\eta^2}{\pi^2 \sqrt{2Q+1}} \left[\pi + 2 \arcsin\left(\frac{Q}{3Q+1}\right) - 4 \arcsin\left(\frac{\rho}{\sqrt{(3Q+1)(2(Q-\rho^2)+1)}}\right) \right]. \end{aligned} \quad (85)$$

The explicit η^2 term is the variance of the online update. Introducing $r = 1 - R$ gives

$$\frac{dr}{d\alpha} = \frac{1-r}{2Q} \frac{dQ}{d\alpha} - \frac{1}{\sqrt{Q}} \frac{d\rho}{d\alpha}. \quad (86)$$

For $Q \gg 1$, $r \ll 1$, and $s = Qr = O(1)$, the large- Q expansion has the form

$$\frac{dQ}{d\alpha} = c(s, \eta) Q^{-1/2} + O(Q^{-3/2}), \quad (87)$$

$$\frac{dr}{d\alpha} = r_3(s, \eta) Q^{-3/2} + O(Q^{-5/2}), \quad (88)$$

where

$$c(s, \eta) = \frac{4\eta}{\pi} \left(\frac{1}{\sqrt{1+2s}} - \frac{1}{\sqrt{2}} \right) + \frac{\sqrt{2}}{\pi^2} \eta^2 J(s), \quad (89)$$

$$r_3(s, \eta) = -\frac{4\eta s}{\pi\sqrt{1+2s}} + \frac{\eta^2}{\pi^2\sqrt{2}} J(s), \quad (90)$$

$$J(s) = \pi + 2 \arcsin \left(\frac{1}{3} \right) - 4 \arcsin \left(\frac{1}{\sqrt{3(1+4s)}} \right). \quad (91)$$

A consistent power law requires $r_3(s_*, \eta) = 0$, which fixes $s_* = \lim_{\alpha \rightarrow \infty} Qr$. Then

$$Q(\alpha) \sim \left[\frac{3}{2} c(s_*, \eta) \alpha \right]^{2/3}, \quad r(\alpha) \sim \frac{s_*}{Q(\alpha)} \sim \alpha^{-2/3}. \quad (92)$$

The binary classification error is

$$\epsilon_g = \frac{1}{\pi} \arccos R = \frac{1}{\pi} \arccos(1-r) \sim \frac{\sqrt{2r}}{\pi}, \quad (93)$$

and hence $\epsilon_g \sim \alpha^{-1/3}$. If the learning rate decays adiabatically, the same reduced structure gives a noise-floor relation $r \sim k\eta/Q$ and leads to $\epsilon_g \sim \alpha^{-(2+\gamma)/6}$ when $\eta \propto \alpha^{-\gamma}$ with $\gamma < 1$. This binary calculation is a useful sanity check and demonstrates similar behavior beyond softmax and cross-entropy loss, but the main paper's results are the multiclass softmax boundary-layer formulas derived above.

E Numerical protocols and additional robustness checks

This appendix summarizes the numerical settings underlying the main figures and records additional robustness checks. The reported observables are the test misclassification rate ϵ_g , the centered margin $D = R - S$, the residual variance $\Delta = Q_{\text{eff}} - D^2$, as well as the test loss \mathcal{L}_g . The total computational cost for all simulations reported in the manuscript was on the order of 10^3 CPU-hours.

For the two main teacher-student validation figures, Figs. 2 and 3, we used the online $K = 3$ softmax teacher-student model at dimension $N = 500$. The teacher vectors were chosen orthonormal with $T_a \cdot T_b/N = \delta_{ab}$, and the student weights were initialized with independent entries $J_{ai} \sim \mathcal{N}(0, 1)$. Each SGD update used a fresh Gaussian input example, and time is reported in macroscopic units $\alpha = \mu/N$. The curves were generated from six independent random seeds. The plotted envelopes show the corresponding seed-to-seed fluctuations around a representative trajectory. For the fixed-learning-rate comparison in Fig. 2, the theoretical prediction uses the full asymptotic prefactor: the boundary density c_K was evaluated numerically, and for each fixed learning rate the residual variance floor Δ_* was obtained by numerically solving $2\Delta_* = \eta \mathcal{B}(\Delta_*)$, with \mathcal{B} defined in Eq. (11). For the schedule experiment in Fig. 3, the learning-rate family was $\eta(\alpha) = \eta_0(1 + \alpha/\alpha_0)^{-\gamma}$, with $\eta_0 = 2.0$, $\alpha_0 = 200.0$, and the plotted exponents $\gamma \in \{0, 0.5, 1\}$. The generalization error ϵ_g was estimated by Monte Carlo evaluation on $M = 10^5$ fresh test examples.

E.1 Number of classes: K -dependence

The main-text simulations focus on $K = 3$, while the asymptotic theory is stated for fixed but arbitrary K . We therefore include an explicit K -sweep as a check that the predicted fixed- K boundary-layer

mechanism is not unique to the three-class case. For fixed learning rate, the theory predicts that the exponents are independent of K ,

$$D \sim \alpha^{1/3}, \quad \epsilon_g \sim \alpha^{-1/3}, \quad (94)$$

while the prefactors depend on K through the boundary density c_K and the classification-error constant

$$\Gamma_K = \frac{K(K-1)c_K}{\sqrt{\pi}}. \quad (95)$$

More explicitly,

$$D^3(\alpha) \sim \frac{3Kc_K}{2} \eta \left(\frac{\pi^2}{6} + \Delta_* \right) \alpha, \quad \epsilon_g \sim \Gamma_K \frac{\sqrt{\Delta_*}}{D}, \quad (96)$$

where the fixed-learning-rate noise floor Δ_* is determined by $2\Delta_* = \eta\mathcal{B}(\Delta_*)$ and is independent of K at this leading order.

Figure 6 shows simulations for $K = 5, 20, 50, 100$ at $N = 200$, with fixed learning rates $\eta = 1.0, 0.1, 0.01$ and $\gamma = 0$. The fluctuation envelopes are computed over 6 seeds. Across all tested values of K , the late-time trajectories remain in excellent agreement with the predicted asymptotic structure. The centered overlap follows the $D \sim \alpha^{1/3}$ law, the residual variance approaches the learning-rate-dependent floor, and the generalization error follows the resulting $\epsilon_g \sim \sqrt{\Delta_*}/D$ decay. Increasing K induces a later crossover into the asymptotic regime. This is expected since for larger K , the top teacher fields are closer and the pairwise boundary-layer approximation becomes valid only once the centered margin given by D is large compared to the typical extreme-value scale, $D \gg \sqrt{2 \log K}$. Thus larger K produces longer transients before the fixed- K late-time theory becomes visible.

E.2 Correlated Gaussian inputs

For the correlated-Gaussian robustness check, the input covariance is diagonal with eigenvalues proportional to $i^{-\beta}$ and normalized so that the largest variance is one. Concretely, inputs were generated as $\xi_i = \sqrt{\lambda_i} x_i$, with $x_i \sim \mathcal{N}(0, 1)$ independently and

$$\lambda_i = \left(\frac{a}{a+i} \right)^\beta, \quad i = 0, \dots, N-1, \quad (97)$$

with $a = 10$ in the experiments, so that the largest variance has $\lambda_0 = 1$ and increasing β produces a stronger power-law anisotropy. The teacher vectors were sampled from independent standard-normal entries and then orthogonalized by Gram-Schmidt with respect to the normalized Euclidean inner product, followed by the normalization $T_a \cdot T_b/N = \delta_{ab}$. Thus the covariance spectrum is structured, but the teacher directions are otherwise random with respect to the covariance eigenbasis. The student weights were initialized with independent $J_{ai} \sim \mathcal{N}(0, 1)$, as in the isotropic simulations. The labels are still generated by the teacher. Increasing β creates a structured spectrum and lengthens the transient. The observed late-time behavior remains consistent with the same boundary-layer exponent.

E.3 Whitened feature experiments

The feature experiments use pretrained vision-transformer features as a non-Gaussian test bed [28]. Whitening removes the leading covariance structure, so the experiment probes whether non-Gaussian feature statistics destroy the boundary-layer pattern. Teacher-generated labels are used in the main text because they avoid an early performance floor and allow the late-time regime to remain visible. Real-label runs can reach a floor too early for a clean asymptotic fit, but they are useful as a practical diagnostic.

In these experiments we used CIFAR-5M images [37] and extracted fixed features with the pretrained ViT-B/16 model `google/vit-base-patch16-224-in21k` [28]. Images were passed through the ViT feature extractor and the pooled [CLS] representation was used as the input feature vector. For comparability with the $K = 3$ teacher-student simulations, we restricted the dataset to three CIFAR

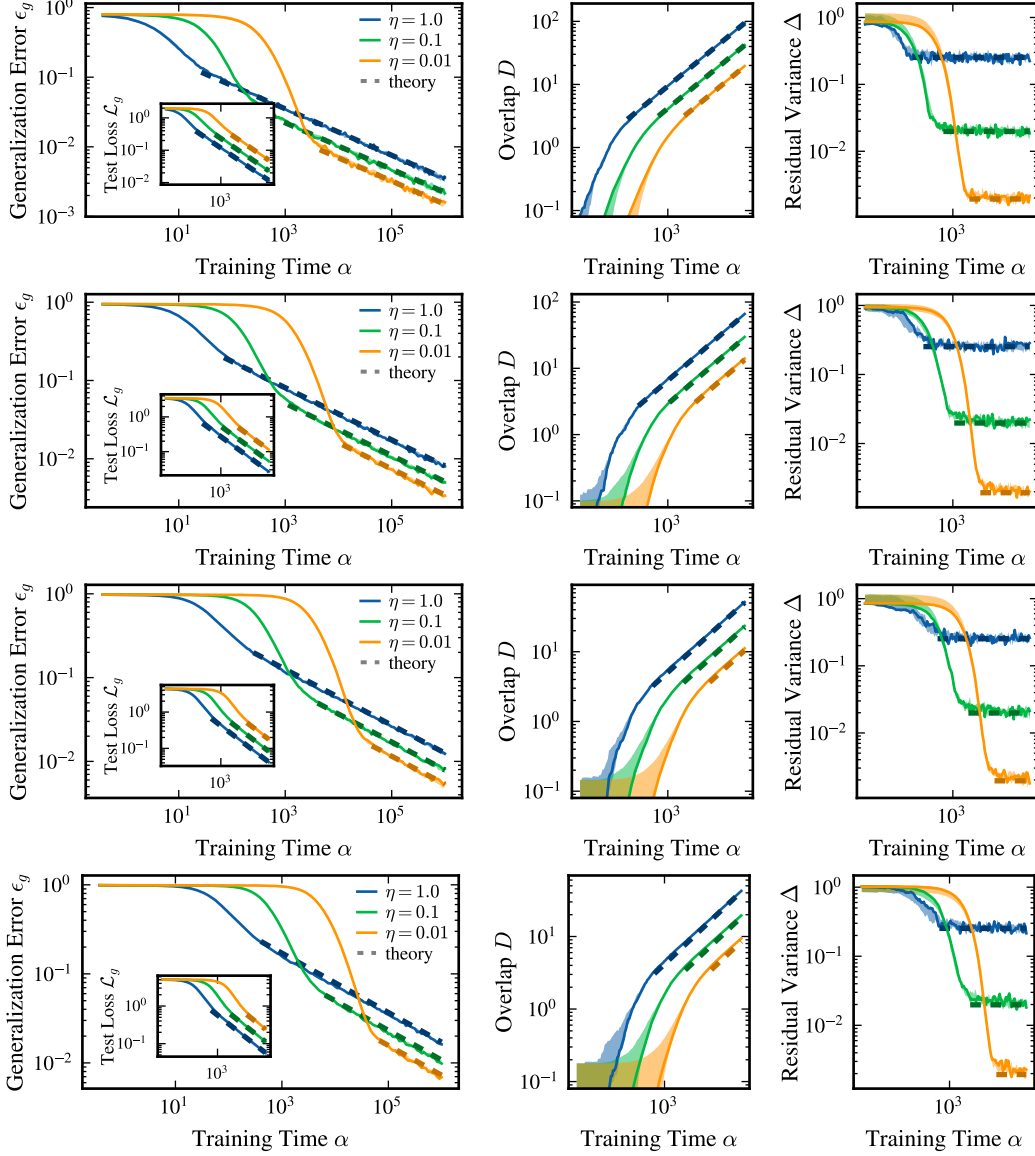


Figure 6: Dependence on the number of classes. Fixed-learning-rate simulations for $K = 5, 20, 50, 100$ (increasing from top to bottom) at $N = 200$, with $\eta = 1.0, 0.1, 0.01$, $\gamma = 0$, and envelopes over 6 seeds. For each value of K , the panels show the generalization error ϵ_g , the centered student-teacher overlap D , and the residual variance Δ . The late-time behavior agrees with the fixed- K boundary-layer prediction: $D \sim \alpha^{1/3}$, Δ approaches the learning-rate noise floor, and $\epsilon_g \sim \alpha^{-1/3}$. Increasing K delays the onset of the asymptotic regime.

classes: airplane, automobile, and horse. This class triple was chosen because, among the tested three-class subsets, it gave one of the lowest apparent irreducible errors when a linear classifier was trained on the ViT features, making it a favorable case for observing a long late-time regime before a real-label floor is reached. Before training the linear readout, we subtracted the empirical feature mean and applied ZCA whitening: if X denotes the matrix of centered ViT features with empirical covariance $C = X^\top X / (n - 1)$, we used the eigendecomposition $C = U\Lambda U^\top$ and transformed the features by $X \mapsto XU(\Lambda + \varepsilon I)^{-1/2}U^\top$, with a small numerical regularizer $\varepsilon = 10^{-5}$. The resulting whitened features have approximately identity empirical covariance, but their distribution remains strongly non-Gaussian. The figures show envelopes over four seeds.

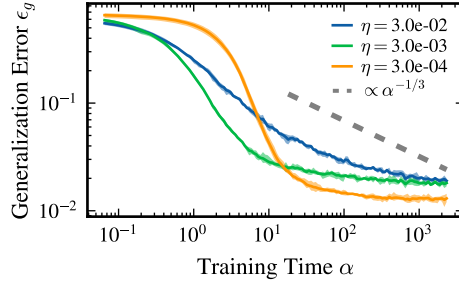


Figure 7: Whitened pretrained-feature experiment with real labels. This run is included as a qualitative practical comparison to the teacher-label experiment in Fig. 5; the real-label performance floor is reached earlier, making it less suitable as a clean asymptotic test.

The readout architecture differs slightly from the analytically normalized teacher-student model. In the ViT-feature experiments we trained a linear layer, $f(x) = Wx$, without the explicit $1/\sqrt{N}$ factor in the logit definition. Consequently the runs used the default smaller PyTorch linear-layer initialization and correspondingly smaller learning rates than in the Gaussian teacher-student simulations. Specifically, for input dimension N , `torch.nn.Linear` initializes both weights and, when present, biases from the uniform distribution $\mathcal{U}(-N^{-1/2}, N^{-1/2})$. The readout was trained with cross-entropy loss using online SGD without momentum, with batch size one. Time was again reported in normalized units as the number of SGD steps divided by the feature dimension.

The numerical evidence should be interpreted conservatively. The asymptotic theory is for isotropic Gaussian inputs in the thermodynamic limit. The correlated-input and whitened-feature experiments show that the mechanism can remain visible under controlled departures, but they do not constitute a theorem for arbitrary feature distributions or real-data classification.